Supporting Information

Fe/Fe_3C@C Nanoparticles Encapsulated in N-Doped Graphene-CNTs Framework as Efficient Bifunctional Oxygen Electrocatalyst for Robust Rechargeable Zn-air Battery

Qichen Wang,[abc] Yongpeng Lei,*[ab] Zhiyan Chen,[c] Nan Wu,[d] Yaobing Wang,*[e] Bing Wang,[d] and Yingde Wang*[d]

Supplemental Figures and Tables

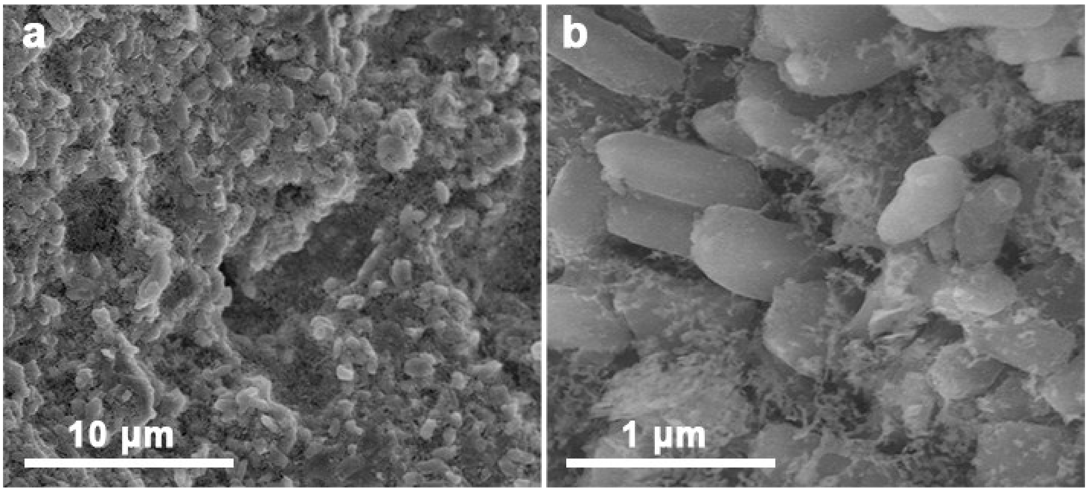

Figure S1. SEM images of product at 550 °C for 4h.

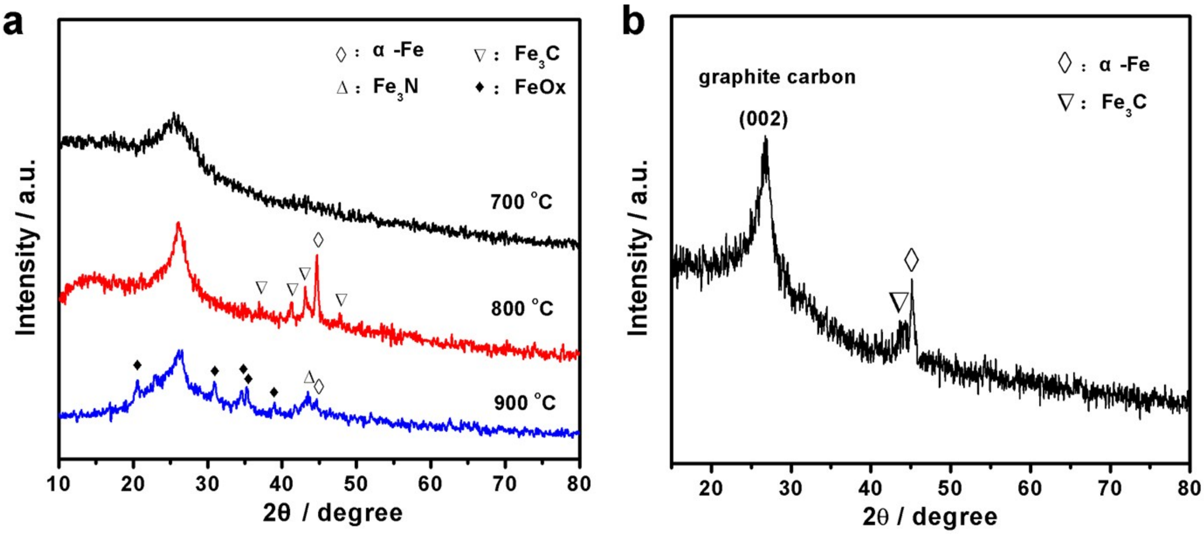

Figure S2. XRD patterns of samples prepared at (a) 700 °C, 800 °C and 900 °C and (b) Fe-BL.

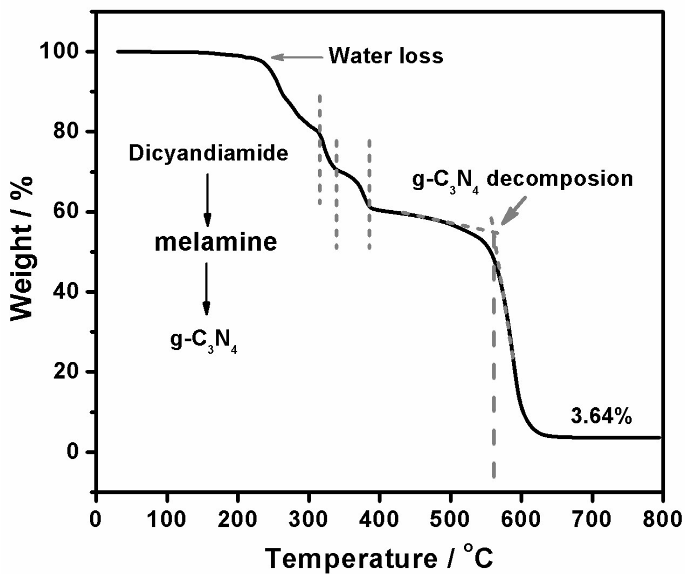

Figure S3. TGA curve of Fe@C-NG/NCNTs.

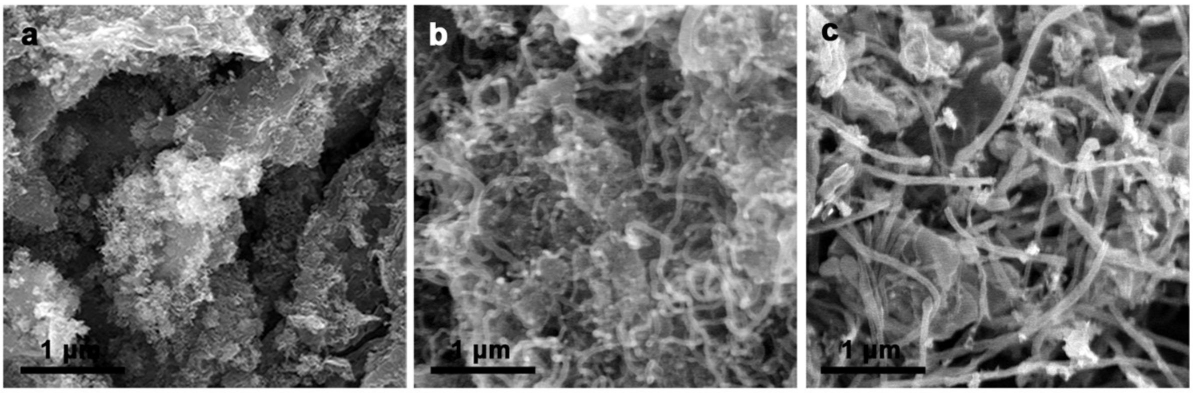

Figure S4. SEM images of samples prepared at (a) 700 °C, (b) 800 °C, (c) 900 °C.

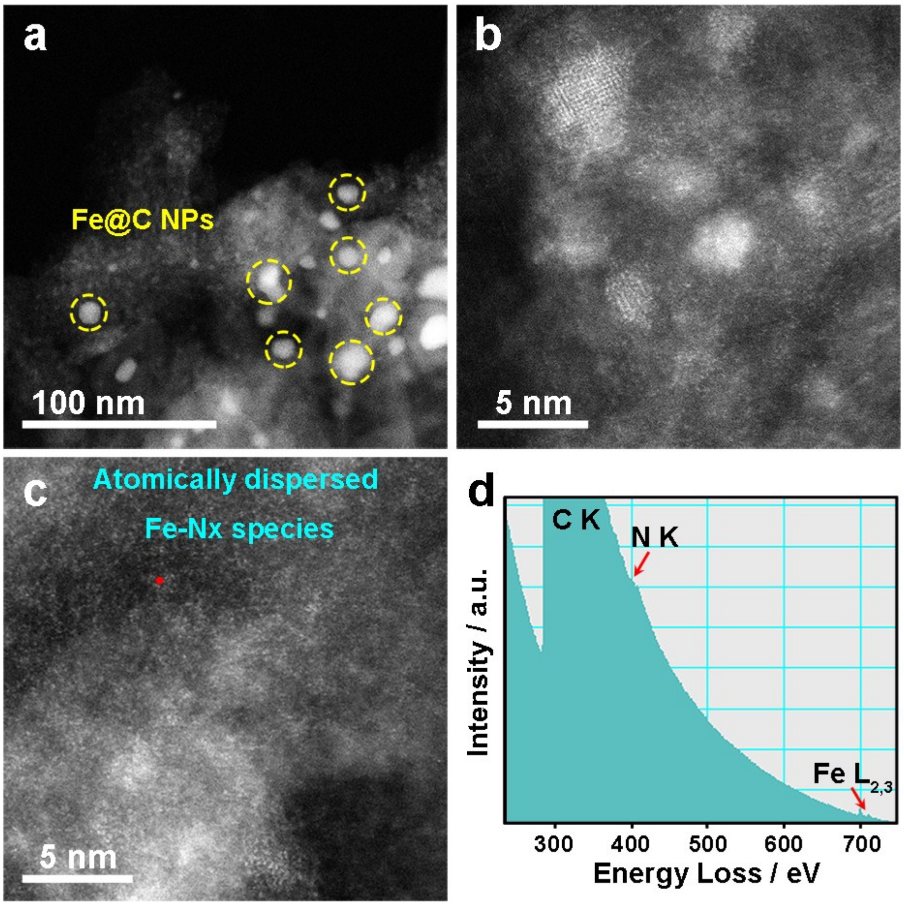

Figure S5. (a-c) HAADF-STEM images, (d) EELS spectrum of Fe@C-NG/NCNTs taken at red spot of HAADF-STEM image.

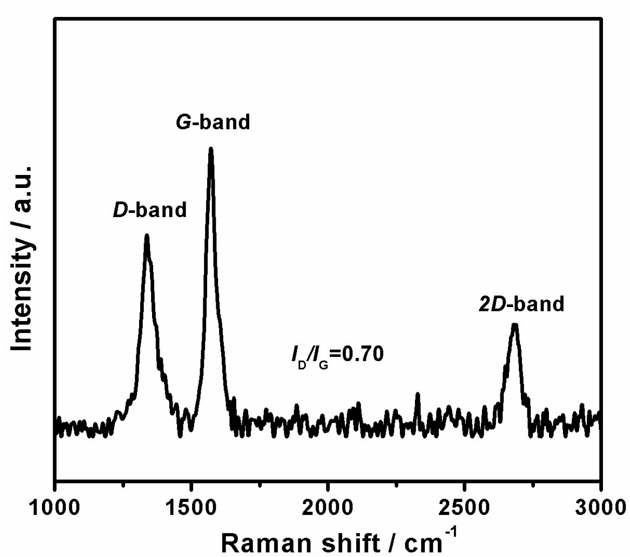

Figure S6. Raman spectra of Fe@C-NG/NCNTs.

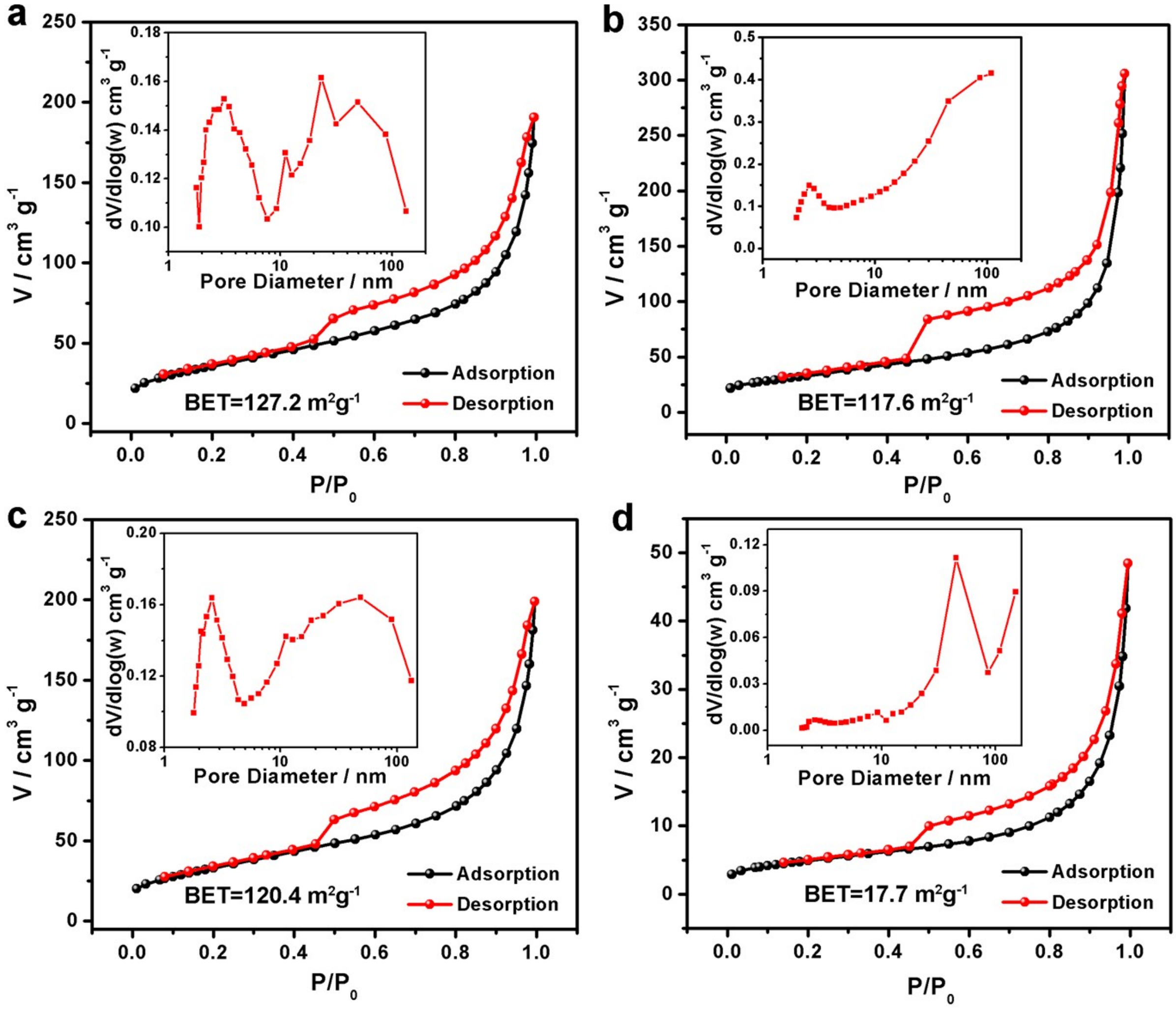

Figure S7. N_2 adsorption/desorption isotherms of samples prepared at (a) 700 °C, (b) 800 °C, (c) 900 °C and (d) comparison sample prepared in absence of SBA-15.

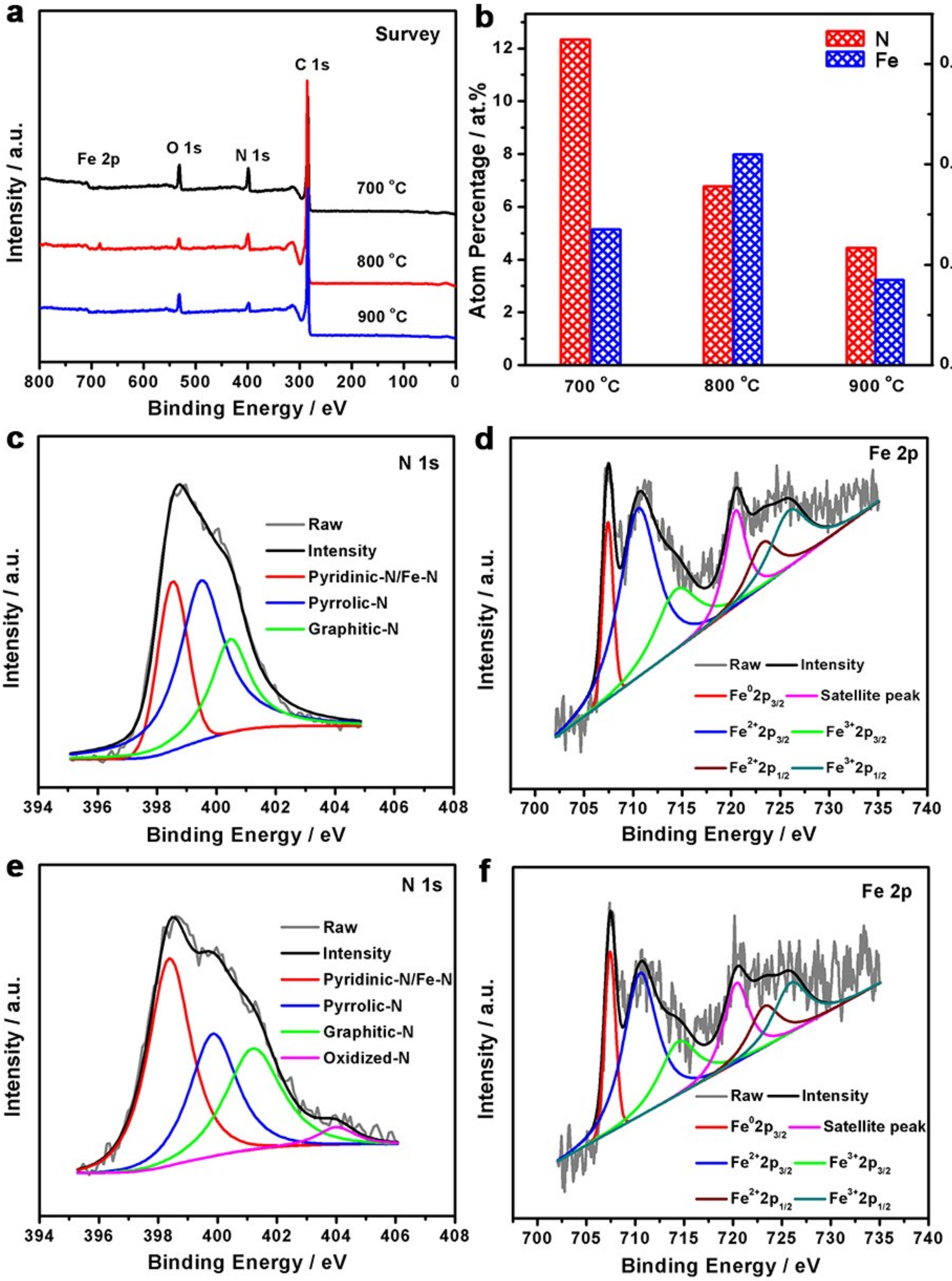

Figure S8. (a) XPS survey spectrum, (b) Comparsion of N and Fe content of samples prepared at 700-900 °C, (c) High-resolution N 1s spectrum and (d) High-resolution Fe 2p spectrum for sample at 700 °C, (e) High-resolution N 1s spectrum and (f) High-resolution Fe 2p spectrum for sample at 900 °C.

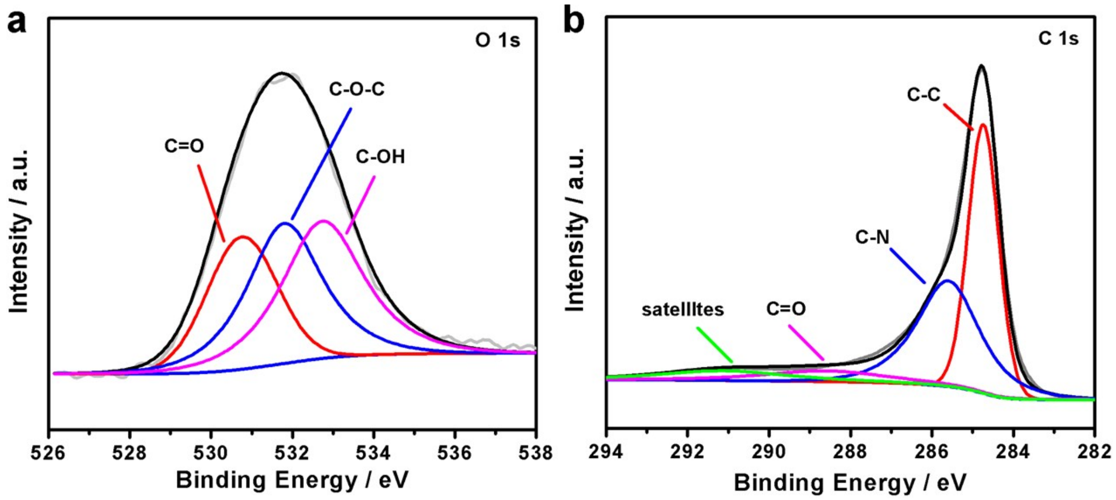

Figure S9. (a) High-resolution O 1s, (b) C 1s XPS spectrum for Fe@C-NG/NCNTs.

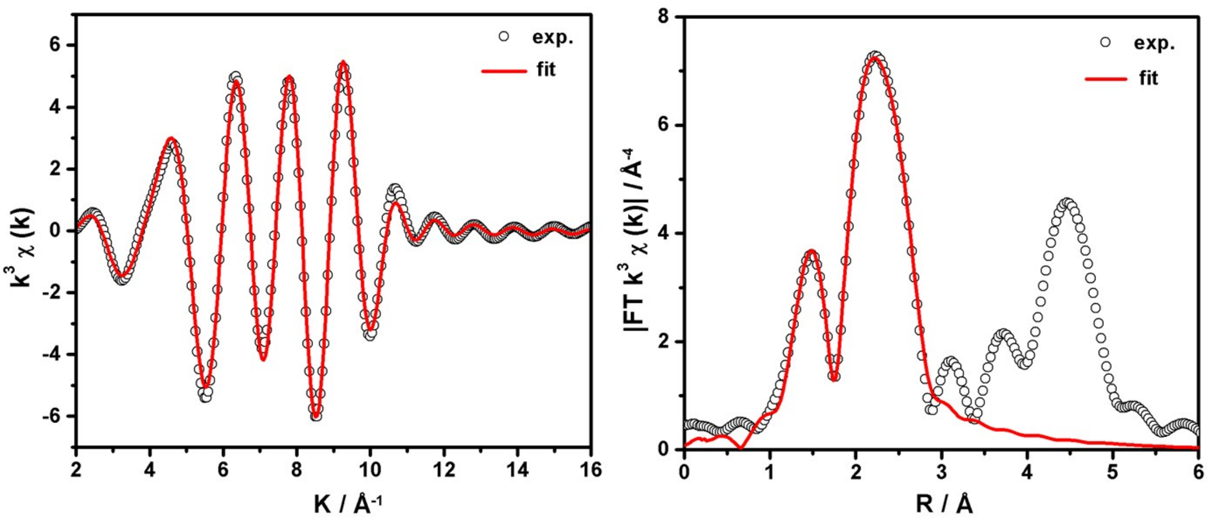

Figure S10. Comparison between simulations and experimental data of (a) Fe K-edge EXAFS spectrum and (b) FT-EXAFS curve for Fe@C-NG/NCNTs.

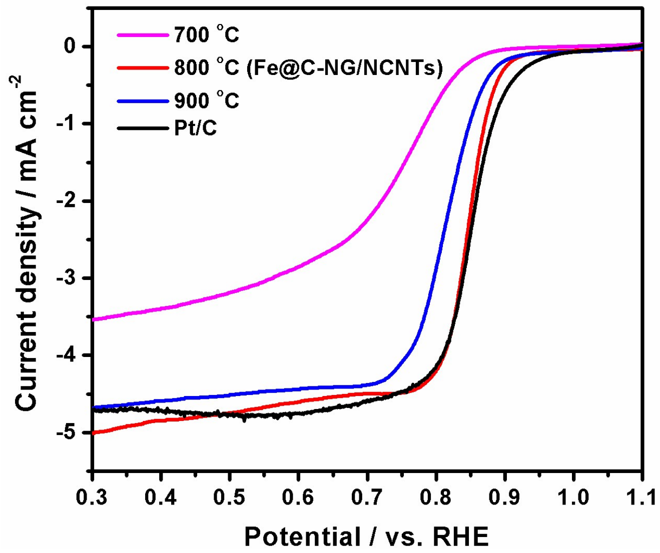

Figure S11. (a) LSV curves of different samples prepared at 700-900 °C and Pt/C at 1600 rpm.

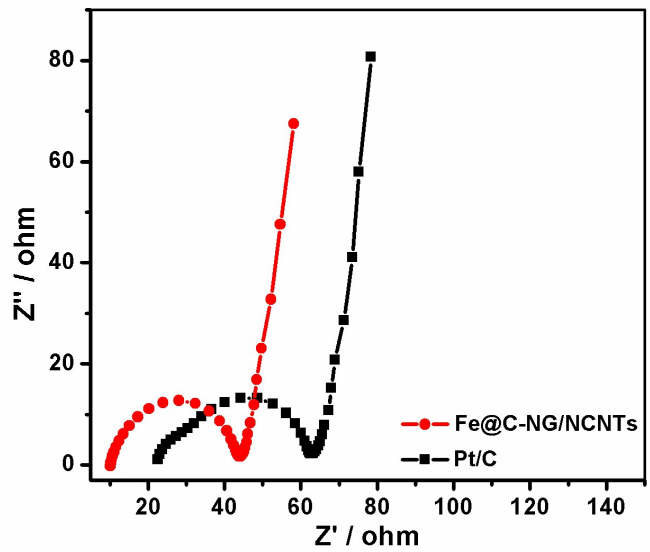

Figure S12. The electrochemical impendence spectroscopy of Fe@C-NG/NCNTs and Pt/C.

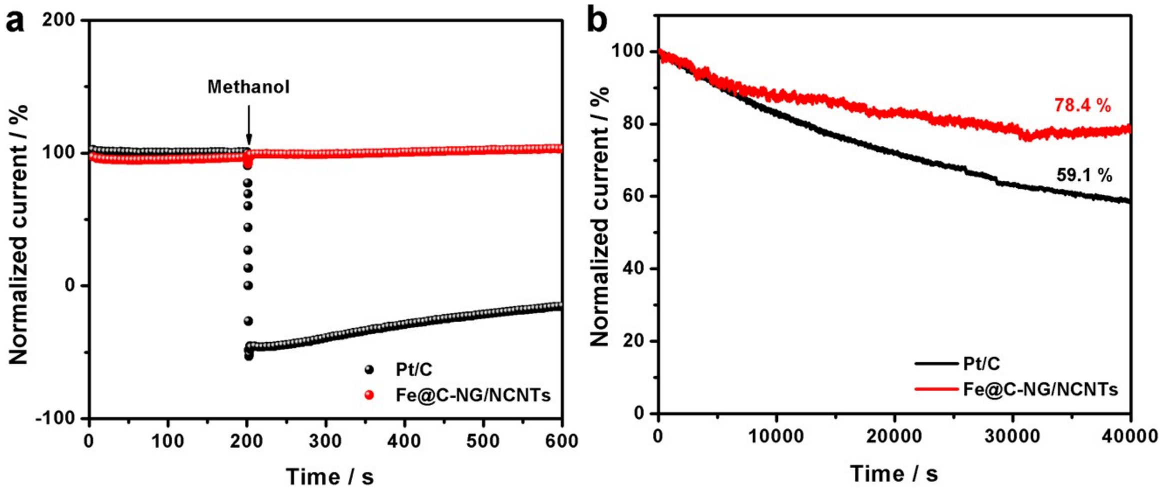

Figure S13. Chronoamperometric response of Fe@C-NG/NCNTs and Pt/C in O_2-saturated 0.1 M KOH to test methanol crossover effect, (b) Long-term stability at 0.8 V.

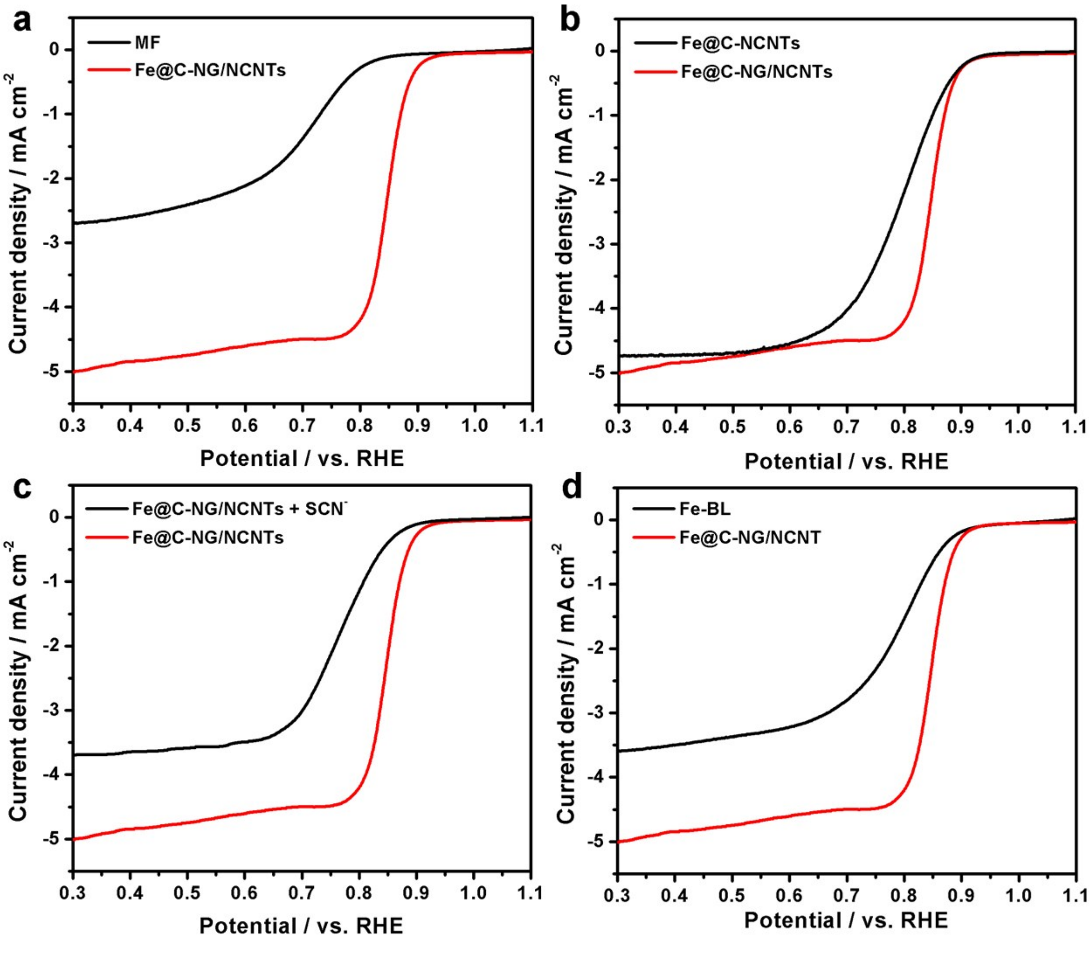

Figure S14. LSV curves of different controlled samples at 1600 rpm.

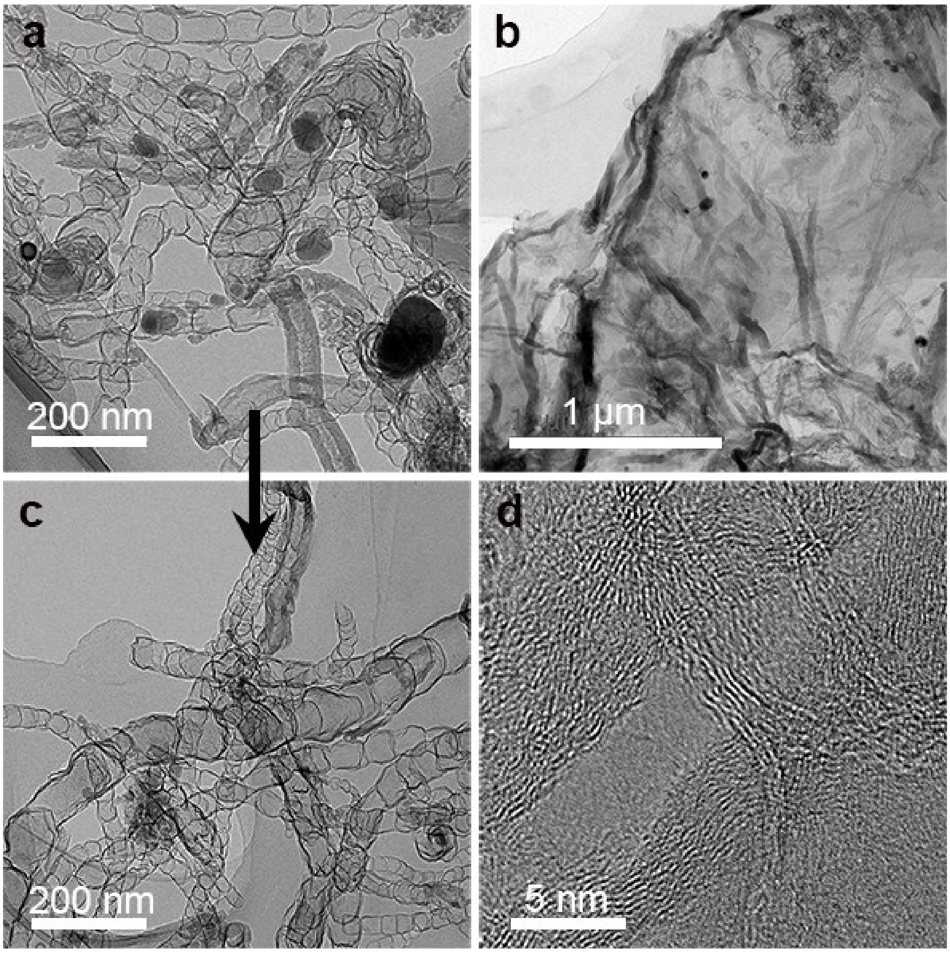

Figure S15. (a) TEM image of Fe@C-NG/NCNTs. (b, c) TEM and (d) HRTEM images of Fe-BL.

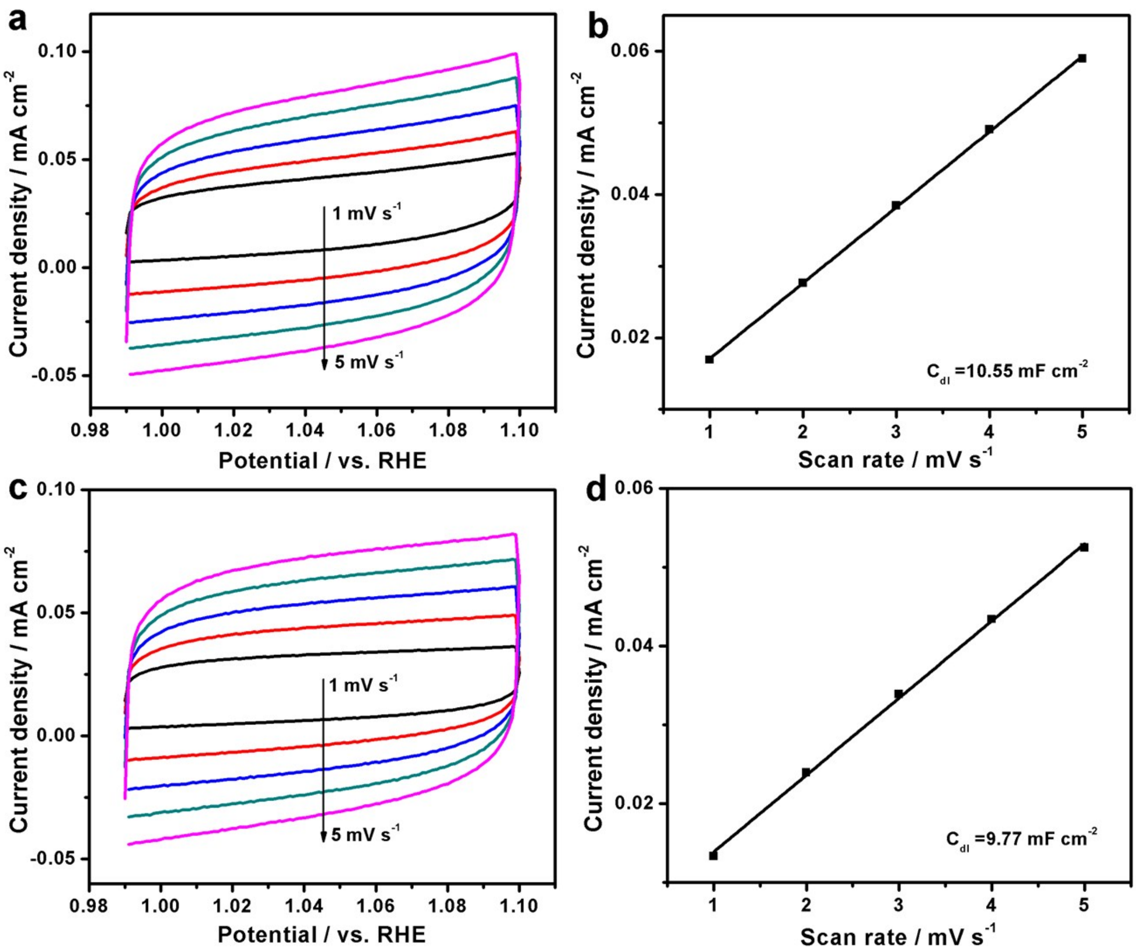

Figure S16. CVs at scan rates of 1, 2, 3, 4 and 5 mV s^{-1} in O_2-satuated 0.1 M KOH and the corresponding current density taken at 1.045 V for (a, b) Fe@C-NG/NCNTs, (c,d) Fe-BL.

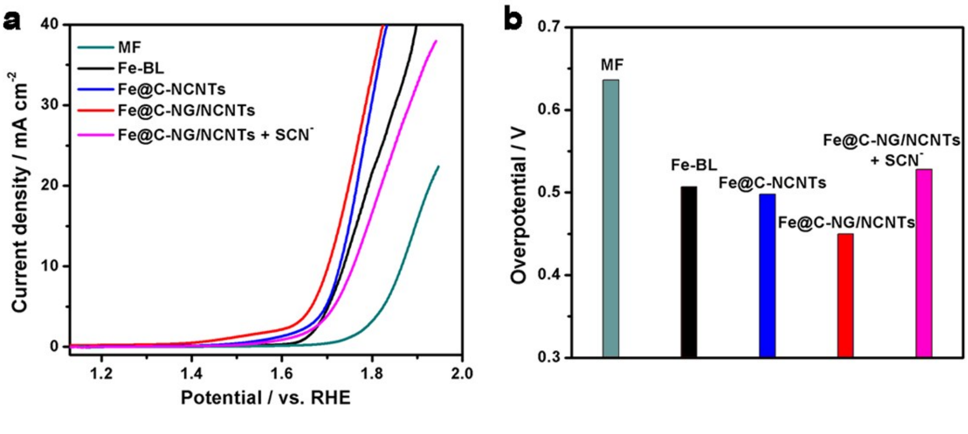

Figure S17. (a) LSV curves of MF, Fe-BL, Fe@C-NCNTs, Fe@C-NG/NCNTs and Fe@C-NG/NCNTs + SCN^- electrode for OER. (b) Overpotential at 10 mA cm^{-2} for MF, Fe@C-NCNTs, Fe-BL, Fe@C-NG/NCNTs and Fe@C-NG/NCNTs + SCN^- electrode.

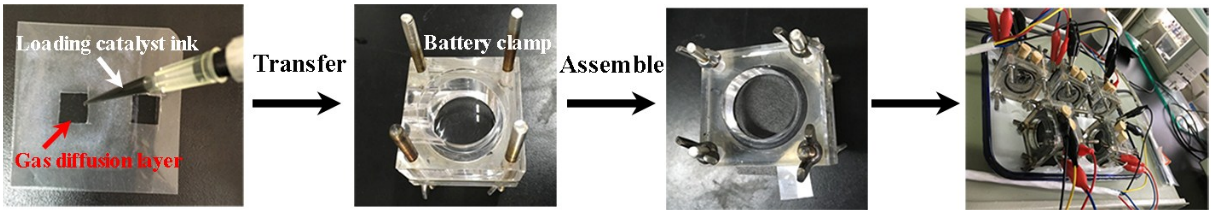

Figure S18. The process of constructing Zn-air batteries.

Q1: Why catalyst obtained at 800 °C shows better activity than 700 °C and 900 °C?

The CNTs was not observed in samples prepared at 700 °C (Figure S4), which may be attributed to that the Fe^{3+} was not reduced to metallic iron by carbothermal reduction at 700 °C. And the corresponded XRD profile showed no Fe-based diffraction peaks (Figure S2). Then CNTs appeared at 800°C may be due to the fact that the Fe^{3+} were reduced to Fe/Fe_3C nanoparticles, thus promoting the rearrangement of carbon atoms during heat treatment. At 900 °C, the diameter of CNTs become much larger. The peaks shift from Fe_3C to Fe_3N and FeO_x. The presence of iron compounds varied with temperature, indicating that the temperature affects the reaction between Fe^{3+} and carbon thus would affect the final electrochemical performance. Interestingly, the N_2 adsorption/desorption isotherm in Figure S7 for three samples shows the meso-macroporous feature, similar BET surface area and pore volume. On the other hand, atomically dispersed Fe-N_x species are able to act as highly active sites. Based on XPS analysis in Figure S8, sample prepared at 800 °C shows the highest Fe content. In other words, Fe@C-NG/NCNTs prepared at 800 °C has the highest content of Fe-N_x active sites among all samples. The above mentioned proof could rationally explain that why catalyst obtained at 800 °C shows better activity than 700 °C and 900 °C.

Table S1. Structural parameters extracted from the Fe K-edge EXAFS fitting. (S_0^2=0.85)

Sample	Scattering pair	CN	R(Å)	$\sigma^2(10^{-3}Å^2)$	ΔE_0(eV)	R factor
Fe@C-NG/NCNTs	Fe-N	3.1	1.89	10.3	-1.5	0.0049
	Fe-Fe	4.2	2.44	7.9	-2.1	
Fe foil	Fe-Fe1	8	2.48	5.9	1.2	0.0032
	Fe-Fe2	6	2.85	7.2		
Fe_2O_3	Fe-O1	3	1.93	4.4	0.5	0.0001
	Fe-O2	3	2.09	6.4		

S_0^2 is the amplitude reduction factor; CN is the coordination number; R is interatomic distance (the bond length between Fe central atoms and surrounding coordination atoms); σ^2 is Debye-Waller factor (a measure of thermal and static disorder in absorber-scatterer distances); ΔE_0 is edge-energy shift (the difference between the zero kinetic energy value of the sample and that of the theoretical model). R factor is used to value the goodness of the fitting. * This value was fixed during EXAFS fitting, based on the known structure of Fe metal.

Error bounds that characterize the structural parameters obtained by EXAFS spectroscopy were estimated as N ± 20%; R ± 1%; σ^2 ± 20%; ΔE_0 ± 20%.

Table S2. The comparison of ORR activity of the other noble-metal-free electrocatalysts based materials from previous literatures.

Catalysts	**ORR E_{onset} (V)**	**ORR $E_{1/2}$ (V)**	**OER $E_{j=10\ mA\ cm^{-2}}$**	**Δ E $E_{j=10\ mA\ cm^{-2}}$ - $E_{1/2}$**	**Reference**
Fe@C-NG/NCNTs	0.93	0.84	1.68	0.84	This work!
NC@Co-NGC DSNCs	0.92	0.82	1.64	0.82	*Adv. Mater.* **2017**, *29*, 1700874-1700883.
N-Co_9S_8/G	0.94	0.74	1.64	0.90	*Energy Environ. Sci.*, **2016**, *9*, 1320-1326.
Co-C_3N_4/CNT	0.94	0.85	1.61	0.76	*J. Am. Chem. Soc.* **2017**, *139*, 3336-3339.
Fe@N-C-700	0.97	0.83	1.71	0.88	*Nano Energy* **2015**, *13*, 387-396.
N-GCNT/FeCo-3	1.03	0.92	1.73	0.81	*Adv. Energy Mater.* **2017**, *7*, 1602420-1602431.
NGM-Co	0.88	0.79	1.74	0.95	*Adv. Mater.* **2017**, 29, 1703185-1703191.
Ni_3Fe/N-C	0.95	0.76	1.60	0.84	*Adv. Energy Mater.* **2017**, *7*, 1601172-1601179.
NiO/CoN PINWs	0.89	0.68	1.53	0.85	*ACS Nano.* **2017**, *11*, 2275-2283.
NCNF-1000	0.97	0.82	1.84	1.02	*Adv. Mater.* **2016**, *28*, 3000-3006.

Table S3. Comparison the performance of zinc-air batteries reported.

Catalysts	Open-circuit voltage (V)	Maximum power density (mW cm^{-2})	Specific capacity (mAh g^{-1})	Energy density (Wh kg^{-1})	Reference
Fe@C-NG/NCNTs	1.44	146.5	682	765	This work!
NCNT/$Co_xMn_{1-x}O$	1.35	102.7	581	695	*Nano Energy* **2016**, *20*, 315-325.
NC@Co-NGC DSNC	1.45	109	565	510	*Adv. Mater.* **2017**, *29*, 1700874-1700883.
CoZn-NC-700	1.42	152	578	694	*Adv. Funct. Mater.* **2017**, 27, 1700795-1700808.
NiFe@NC_x	1.36	77	584	732	*ACS Catal.* **2016**, *6,* 6335-6342.
Ni_3Fe/N-C			528	634	*Adv. Energy Mater.* **2017**, *7*, 1601172-1601179.
$ZnCo_2O_4$/N-CNT	1.47	82.3	428	595	*Adv. Mater.* **2016**, *28*, 3777-3784.
Fe-N-CNFs	1.50		614	760	*Angew. Chem. Int. Ed.* **2015**, *54*, 8179-8183.
NiO/CoN PINWs	1.46	79.6	648	836	*ACS Nano.* **2017**, *11*, 2275-2283.
NGM-Co		152	750	820	*Adv. Mater.* **2017**, 29, 1703185-1703191.
NCNF-1000	1.48	185	626	776	*Adv. Mater.* **2016**, *28*, 3000-3006.